# Coarse-Grained Simulation Studies of Peptide-Induced Pore Formation

Gregoria Illya*† and Markus Deserno*‡
*Max-Planck-Institute for Polymer Research, Mainz, Germany; †Department of Chemistry, Technical University of Darmstadt, Darmstadt, Germany; and ‡Department of Physics, Carnegie Mellon University, Pittsburgh, Pennsylvania

ABSTRACT We investigate the interactions between lipid bilayers and amphiphilic peptides using a solvent-free coarse-grained simulation technique. In our model, each lipid is represented by one hydrophilic and three hydrophobic beads. The amphiphilic peptide is modeled as a hydrophobic-hydrophilic cylinder with hydrophilic caps. We find that with increasing peptide-lipid attraction the preferred state of the peptide changes from desorbed, to adsorbed, to inserted. A single peptide with weak attraction binds on the bilayer surface, while one with strong attraction spontaneously inserts into the bilayer. We show how several peptides, which individually bind only to the bilayer surface, cooperatively insert. Furthermore, hydrophilic strips along the peptide cylinder induce the formation of multipeptide pores, whose size and morphology depend on the peptides' overall hydrophilicity, the distribution of hydrophilic residues, and the peptide-peptide interactions. Strongly hydrophilic peptides insert less readily, but prove to be more destructive to bilayer integrity.

## INTRODUCTION

The interaction between biological membranes and many naturally produced peptides, such as gene-encoded antimicrobial peptides (APs) and toxins, have been extensively studied for the last few decades. Numerous APs have been isolated from different multicellular organisms, for instance the magainin family of the African frog *Xenopus laevis* (1,2), melittin (which is the cytolytic peptide of bee venom) (3), and alamethicin of the fungus *Trichoderma viridae* (4). Antimicrobial peptides provide a protection against microbial invasion and are usually amphipathic and cationic. They are known to permeabilize the lipid membranes surrounding the pathogens, thus causing cell death.

A universal feature of APs is the cooperative concentration dependence of their activities (5–7). Due to its amphipathic structure (illustrated for the case of the $\alpha$-helical magainin 2 in Fig. 1, *a* and *b*), a single peptide embeds in the headgroup region of the lipid bilayer (the interface state) (6,8–12). As the peptide concentration increases beyond a threshold value, the peptide molecules may remain in the interface state or subsequently change into the transmembrane state, where they aggregate into transmembrane nanometer-sized pores that lead to cell death (6,8–11,13,14).

Despite the growing interest in APs, the mechanism involved in bilayer pore formation or rupture is not very well understood. Three modes of action have been proposed to date—termed the carpet, barrel-stave, and toroidal models. In the carpet model (7,15), peptides initially bind to and cover the surface of the bilayer. The electrostatic interaction between the peptide and the lipid headgroup imposes a strain in the bilayer and permeation is induced. In the barrel-stave model (16,17), peptides bind to the bilayer and oligomerize, and these oligomers insert into the bilayer and form a transmembrane channel. The hydrophobic surface of the peptide faces the hydrophobic core of the bilayer and the hydrophilic surface points inward to create a hydrophilic pore. In the toroidal model (18,19), peptides bind and interact with lipid headgroups, imposing a positive curvature strain on the bilayer such that a pore forms. Its rim-region is stabilized by the peptides without being fully covered by them as in the barrel-stave model.

While significant progress has been made concerning molecular modeling of AP adsorption onto and insertion into a bilayer (20), the known cooperative nature of their action implies that the interplay of many such peptides needs to be studied to understand the origin of their cytotoxicity. For computational feasibility this cannot be accomplished on the atomistic level, therefore various coarse-grained simulational approaches have recently been undertaken (21–26). In this work, we also approach the problem from this opposite end of resolution and use a highly simplified model for membranes and APs to treat a variety of generic questions concerning their cooperative behavior. We are particularly concerned with the problem how 1), the overall balance between hydrophilic and hydrophobic residues; and 2), their spatial distribution on the peptide surface influences geometric properties of the peptide aggregates, such as their size and structure. In other words, rather than aiming at an accurate representation of one specific AP, we focus on overall features shared by many classes of APs. Our results should therefore be seen as generic modes of behavior whose detailed ramifications will depend on finer scale peptide structure.

## SIMULATION MODELS

### Membrane

Our coarse-grained (CG) membrane simulations (see (27,28) for recent reviews on CG membrane approaches) are based on the coarse-grained lipid

*Submitted February 11, 2008, and accepted for publication July 11, 2008.*

Address reprint requests to Markus Deserno, Tel.: 412-268-4401; E-mail: deserno@andrew.cmu.edu.

Editor: Klaus Schulten.


0006-3495/08/11/4163/11 $2.00

doi: 10.1529/biophysj.108.131300

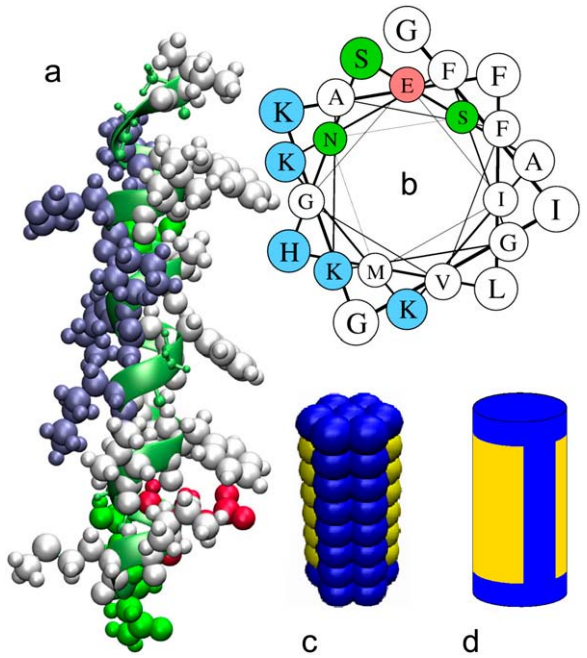


FIGURE 1 (*a*) Atomic structure of magainin 2 (2), a typical $\alpha$-helical antimicrobial peptide. Hydrophilic side chains are shown as dark (basic, *blue*; acidic, *red*; neutral, *green*), others are light-colored. The amino-acid sequence is GIGKFLHSAKKFGKAFVGEIMNS, and its helical wheel representation in panel *b* illustrates clearly the strong hydrophilic/hydrophobic asymmetry, which manifests in a hydrophilic strip running down one side of the peptide. When constructing our coarse-grained peptide from six concentric layers of bead-chains around a central chain, we account for this distinct morphological feature as illustrated in the actual $P_8^2$ peptide (eight-beads-long, two hydrophilic strips) shown in panel *c* and the simplified sketch in panel *d* (*dark color* is again hydrophilic, *light color* is hydrophobic).

model recently proposed by Cooke et al. (29,30). Each lipid consists of linearly connected beads, one head bead and several tail beads. In the absence of explicitly modeled solvent, suitable cohesive interactions between the tails robustly induce self-assembly into fluid bilayer membranes over a wide range of few tuning parameters (see (31) for a recent review on solvent-free membrane simulation approaches). Their large-scale properties faithfully reflect those of real lipid bilayers (30,32,33). Mesoscopic length- and time-scales become accessible, permitting the study of mesoscopic questions such as, for instance, membrane curvature-mediated aggregation and vesiculation of bilayer-bending proteins (34). Details of the model implementation can be found in the literature (29,30). While the original Cooke model used two tail beads, we use three in this study, thereby permitting a slightly higher spatial resolution across the bilayer. The unit of energy is the cohesive potential depth $\varepsilon$. The strength of lipid cohesion can be tuned by the range of interaction, $w_c$, and within the fluid phase, a larger $w_c$ also implies a stronger cohesion, smaller area per lipid, higher lipid order, and larger bending modulus. Using the tail bead diameter $\sigma$ as our unit of length, we will quote the cohesion length in its dimensionless form $\tilde{w}_c = w_c/\sigma$. All beads have the same mass, $m$. This permits the definition of a coarse-grained time unit $\tau = \sigma\sqrt{m/\varepsilon}$.

## Peptides

We represent a coarse-grained $\alpha$-helical peptide by a cylinder composed of CG beads, similar in spirit to Venturoli et al. (24) or Brannigan and Brown (25). Six straight chains of beads of diameter $\sigma$ surround a seventh center-chain (see Fig. 1). Neighboring horizontal, vertical, and diagonal beads are linked by harmonic potentials of the form $(1/2)k(r - r_0)^2$ with $k = 200\,\varepsilon$ and $r_0 = 1.2\,\sigma$. The diagonal bonds are used to prevent the molecule from twisting. They have the same resting length $r_0 = 1.2\,\sigma$ as the straight bonds and are therefore under compression, while, simultaneously, the straight bonds are expanded to a resulting equilibrium length of $\sim 1\,\sigma$. Hydrophobic beads of the peptide interact with lipid tail beads by the same cohesive potential as the one between lipid tails. In most of the simulations, direct peptide-peptide attractions are turned off. The top and bottom caps of the peptide are constructed from hydrophilic beads and the middle region consists of hydrophobic beads, with the exception of $n$ adjacent hydrophilic strips. We use peptides with a length of eight beads (denoted by $P_8^n$, which match to the bilayer thickness) and peptides with a length of six beads ($P_6^n$, which are shorter than the bilayer thickness) to study hydrophobic mismatch on the system as well. Fig. 1 illustrates a $P_8^2$ peptide, i.e., one having length 8 and two hydrophilic strips extending down the cylinder side connecting the caps. As can be seen, this captures the essential amphiphilic nature of typical $\alpha$-helical antimicrobial peptides, such as the ones from the magainin family (1,2). Once in a transmembrane configuration, the diffusion constant of peptides is $\sim 0.01\,\sigma^2/\tau$, showing that they diffuse approximately three times slower than the lipids.

## Coarse-grained units

In the following, we will mostly use the coarse-grained units $\sigma$, $\varepsilon$, and $\tau$ to express length, energy, and time, respectively. This renders our results independent of specific assumptions one invariably needs to make for a mapping to real units. However, for the sake of clarity, let us briefly illustrate a particular way to establish a connection.

*Length*. The CG bilayer thickness, defined to be the difference between the average lipid head bead positions in the upper and lower monolayers, was measured at $\sim 6.5\,\sigma$. Equating this with the transbilayer phosphate-phosphate distance of 4 nm in a real 1,2-dipalmitoyl-*sn*-glycero-3-phosphatidylcholine lipid membrane (35) shows that $\sigma = 0.6$ nm.

*Energy*. In most of our simulations we chose a temperature $T$ according to $k_BT = 1.7\,\varepsilon$. Let us demand that this $T$ should correspond to body temperature. Since then the thermal energy unit is $k_BT_{\text{body}} \simeq 310\text{K} \times 1.38\times10^{-23}\text{J/K} \simeq 4.28\times10^{-21}\text{J} \simeq 0.62\text{kcal/mol}$, we find in this case $\varepsilon \simeq 0.36\,\text{kcal/mol}$.

*Time*. Mapping time is a bit more subtle than length and energy. The straightforward approach would be to use $\tau = \sigma\sqrt{m/\varepsilon}$ and complement the (now) known values for $\sigma$ and $\varepsilon$ by the mass of a coarse-grained bead. The lipid 1,2-dipalmitoyl-*sn*-glycero-3-phosphatidylcholine for instance has a molecular weight of 734, giving $m \approx (1/4) \times 734 \times 1.66 \times 10^{-27}\text{kg} \approx 3.05 \times 10^{-25}\text{kg}$. The thus-obtained time mapping $\tau \approx 6.6$ ps correctly describes the dynamics of the CG system and, in particular, is appropriate for instantaneous dynamic observables such as velocities and, therefore, the kinetic energy, whose value must satisfy the equipartition theorem. However, we are not interested in the dynamics of a fictitious CG system but in the dynamics of the real lipid system—and it is very important to appreciate that these two are different (36,37). Due to the reduction of degrees of freedom and the concomitant elimination of the molecular friction that they cause, the CG system moves significantly faster through phase space than its atomistic counterpart. A very common choice to quantify the associated speedup factor $f_\tau$ is to look at the process of diffusion as the prototypical long-time Brownian dynamic observable. Notice that for the observables of interest in CG simulations this is generally the relevant dynamics based on which one will judge, for instance, equilibration. A typical diffusion constant for phospholipids is $D \simeq 1\,\mu\text{m}^2/\text{s}$, and in simulations of our CG model, we find $D \simeq 0.03\sigma^2/\tau$. This would imply the rough mapping $\tau \simeq 10$ ns, which is a factor $f_\tau \simeq 1500$ faster than the instantaneous time mapping. While the basis underlying these two different dynamic scales is clear, the notation is now awkward because $\tau$ is already defined. To remain consistent with the standard terminology of time mapping in simulations (particularly, atomistic ones), we continue to denote by $\tau = \sigma\sqrt{m/\varepsilon}$ the instantaneous timescale connected to the actual CG simulation (with the implied mapping $\tau \approx 6.6$ ps).

Next to this, we will also define an effective long time unit $\tau_{\text{eff}} = f_\tau \tau$ (= 10 ns in our case), where the speedup is determined—as described—by matching the long time dynamics of the CG system to the actual physical dynamics of the atomistic system it is, after all, supposed to describe. Since for our work it is exclusively the long time regime that is physically relevant, we will always include the speedup $f_\tau \simeq 1500$ when mapping timescales.

## Simulation procedures

We perform molecular dynamics (MD) simulations using the package ESPResSo (38). The time step is set to $\delta t = 0.005\ \tau$. Temperature control is achieved by a Langevin thermostat (39) with friction constant $\Gamma = \tau^{-1}$. A cuboidal simulation box, with lengths $L_x = L_y$ and $L_z$ subject to periodic boundary condition in all three directions, was used. Initially 4000 lipids were preassembled into a flat bilayer spanning the square $xy$ plane, giving a side length of $L_x \approx 53\ \sigma$. Then, 40 peptides were placed in a rectangular lattice at a distance of 4 $\sigma$ above the bilayer. The lateral tension was kept at zero via a modified Andersen barostat (40), allowing simultaneous box resizing in $x$- and $y$-dimensions, with a box friction $\Gamma_{\text{box}} = 10^{-4}\ \tau^{-1}$ and a box mass $Q = 5 \times 10^{-4}\ m$. Visualization of simulation snapshots were done with VMD (41).

Measured results for observables (such as box sizes, pair correlation functions, etc.) were always averaged over three independent runs over the timescales indicated in the text. When we discuss mechanisms of localized processes (e.g., peptide insertion), we describe a sequence of events that appeared typical, judged from the observation of repeated instances of such a process over three independent simulation runs.

# RESULTS

## Fluid bilayer properties

We set the cohesive attraction range between hydrophobic beads to $\tilde{w}_c = 1.6$ and the simulation temperature to $k_B T = 1.7\ \varepsilon$. Under these conditions, lipids self-assemble into fluid bilayers with a bending rigidity $\kappa \approx 20\, k_B T$, as we determined by measuring the tensile force $F$ along cylindrical bilayer tubes of radius $R$, using $\kappa = FR/2\pi$ (33). Lipids in the fluid phase are, on average, oriented parallel to the bilayer normal; more quantitatively, the orientational order parameter $S = (1/2)\langle 3(\boldsymbol{a}_i \cdot \boldsymbol{n})^2 - 1\rangle_i \approx 0.6$, where $\mathbf{a}_i$ is the unit vector along the $i^{\text{th}}$ lipid and $\boldsymbol{n}$ is the average bilayer normal.

## Single peptides

Let us begin by presenting the interaction of single peptides with a fluid bilayer. The peptide-lipid attraction was varied from $\tilde{w}_c = 1.4$ (weak) to $\tilde{w}_c = 1.8$ (strong) for $P_6^2$ and $P_8^2$ peptides. All single-peptide simulations were run for 30,000 $\tau$ ($\sim$300 $\mu$s).

### *Insertion threshold*

$P_8^2$ peptides with a peptide-lipid attraction of $\tilde{w}_c = 1.4$ (initially placed 4 $\sigma$ above the bilayer) do not bind the bilayer but dissolve in the bulk. Increasing the interaction strength to $\tilde{w}_c = 1.5$, the peptide only binds to the surface of the upper monolayer. A few lipids attach to it by orienting approximately perpendicular to the bilayer normal (see Fig. 2), but

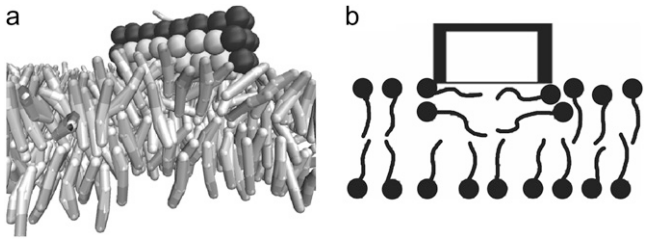


FIGURE 2 (*a*) Snapshot of a single weakly binding $P_8^2$ peptide adsorbing onto the bilayer surface ($\tilde{w}_c = 1.5$). (*b*) Sketch of the concomitant bilayer deformation.

the peptide does not insert into the membrane during the total simulation time. In contrast, when this peptide is initially placed inside the bilayer, with its long axis parallel to the bilayer normal, it remains in the bilayer. This points toward a kinetic barrier for this peptide to change from a bound to an inserted state. As the peptide-lipid attraction is increased to $\tilde{w}_c = 1.6$, a peptide initially placed flat above the bilayer first binds and subsequently inserts spontaneously into the bilayer within a mere 1250 $\tau$ (see Fig. 3). In this case, the peptide first occupies some space in the top monolayer and then rearranges the lipids such that the head beads of some lipids surrounding the peptide face its hydrophilic strip (see sketch in Fig. 3). This structure facilitates spontaneous peptide insertion. We found that, besides a sufficiently strong lipid-peptide attraction, the presence of hydrophilic caps at both ends is necessary to rearrange the lipids into a structure that facilitates the transmembrane peptide insertion.

Since $P_6^2$ peptides contain fewer hydrophobic residues, they need a correspondingly stronger lipid-peptide attraction

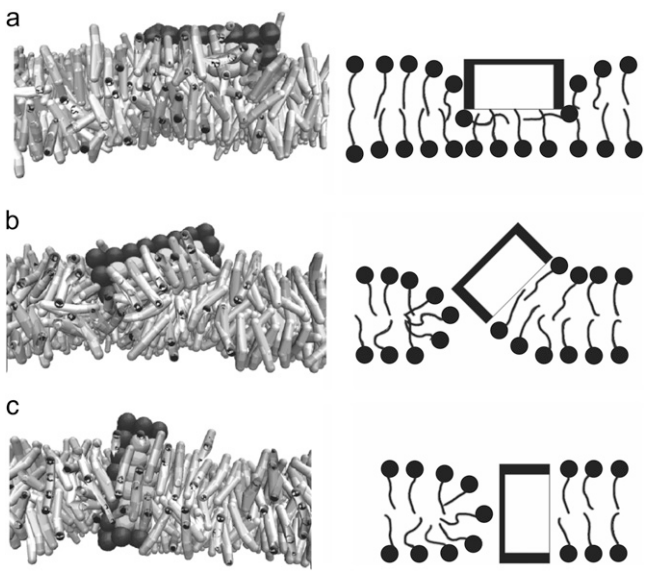


FIGURE 3 Sequence showing a strongly binding $P_8^2$ peptide spontaneously inserting into the bilayer ($\tilde{w}_c = 1.8$). The snapshots were taken at (*a*) 250 $\tau$, (*b*) 750 $\tau$, and (*c*) 1250 $\tau$. The local disturbance is again illustrated on the right.

to insert spontaneously into the membrane. Tables 1 and 2 show the state of $P_6^2$ and $P_8^2$ peptides at two different temperatures. For the $P_6^2$ peptide at peptide-lipid attraction $\tilde{w}_c = 1.6$ and $k_BT = 1.9\ \varepsilon$, the peptide, several times, inserts temporarily into the membrane for a duration of $\Delta t \approx 5000\ \tau$, indicating that, in this case, the barrier separating the two states is small enough to be overcome during a simulation.

### *Energy scales*

How realistic are the energy scales in our CG simulations? Let us picture the peptide as a cylinder that imposes a distance of nearest approach to surrounding lipids of $\sqrt{3}\,\sigma$. A $P_8^2$-peptide then has a height of $6\,\sigma$, and two-thirds of its surface are hydrophobic, giving a total hydrophobic area of $A_h \simeq (2/3) \times 2\pi(\sqrt{3}\,\sigma) \times 6\,\sigma \approx 43.5\sigma^2 \simeq 16\,\text{nm}^2$. Taking a hydrophobic surface free energy density of 25 cal/(mol Å$^2$) (42), this gives a total hydrophobic free energy of insertion of ~40 kcal/mol. The energy of binding measured in our simulation for the $P_8^2$ peptide with $\tilde{w}_c = 1.5$—the one at the brink of insertion—is $(160 \pm 2)\varepsilon = 60$ kcal/mol. Since the lipids surrounding the cylinder are also locally compacted (see below, as well as the literature (21,22)), their entropy is reduced, implying that the free energy of insertion is smaller than the energy. Considering furthermore the considerable ambiguity involved in defining surface areas and mapping length scales, we conclude that the energy scales involved in our modeling are very reasonable.

## Cooperative insertion mechanism

As observed in the previous subsection, single peptides with a weak peptide-lipid attraction only bind onto the bilayer surface within the 30,000 $\tau$ time-span of the simulation. However, increasing the concentration of such peptides enables cooperative insertion modes. Stated differently, peptide insertion becomes an autocatalytic process.

Fig. 4 shows a sequence of several $P_6^2$ peptides, which cooperatively insert and subsequently induce the formation of a pore. The attractive interaction between the hydrophobic residues of these peptides and the lipid tails is $\tilde{w}_c = 1.6$—a value at which we have not seen insertion of single peptides. As the starting state, $P_6^2$ peptides were placed close to each other and ~4 $\sigma$ above the bilayer, and they quickly bind on the top monolayer surface after only 250 $\tau$ simulation time. At ~15,000 $\tau$, three peptides come close together and they attract and perturb most of the lipids underneath them. This is followed by a rapid (≈2000 $\tau$) cooperative insertion of all peptides into the bilayer. Indeed, Zemel et al. (14) have recently shown in a theoretical model (based on chain-packing theory) that two surface-bound peptides can attract by means of the bilayer perturbation which they form, and that the emerging dimer causes a stronger membrane deformation. While they also show that insertion can lower the free energy even further, this comparison of initial and final state cannot predict a pathway or a concomitant free energy barrier.

For the case of just two peptides, Fig. 5 provides a simplified illustration of the cooperative insertion mechanism, as

**TABLE 1 $P_6^2$ peptide states for four values of the peptide-lipid attraction and two temperatures**

| $w_c/\sigma$ | $k_BT = 1.7\ \varepsilon$ | $k_BT = 1.9\ \varepsilon$ |
|---|---|---|
| 1.5 | s | s |
| 1.6 | b | b/i |
| 1.7 | i | i |
| 1.8 | i | i |

State *s* represents stray peptides. State *b* represents an interfacially bound peptide whose direction is parallel to the bilayer plane. State *i* represents a spontaneously inserted peptide whose direction is perpendicular to the bilayer plane. The term *b/i* indicates that, during the simulation time, the peptide several times switched between the *b* and the *i* states.

**TABLE 2 $P_8^2$ peptide states for five values of the peptide-lipid attraction and two temperatures**

| $w_c/\sigma$ | $k_BT = 1.7\ \varepsilon$ | $k_BT = 1.9\ \varepsilon$ |
|---|---|---|
| 1.4 | s | s |
| 1.5 | b | i |
| 1.6 | i | i |
| 1.7 | i | i |
| 1.8 | i | i |

The notation is identical to Table 1.

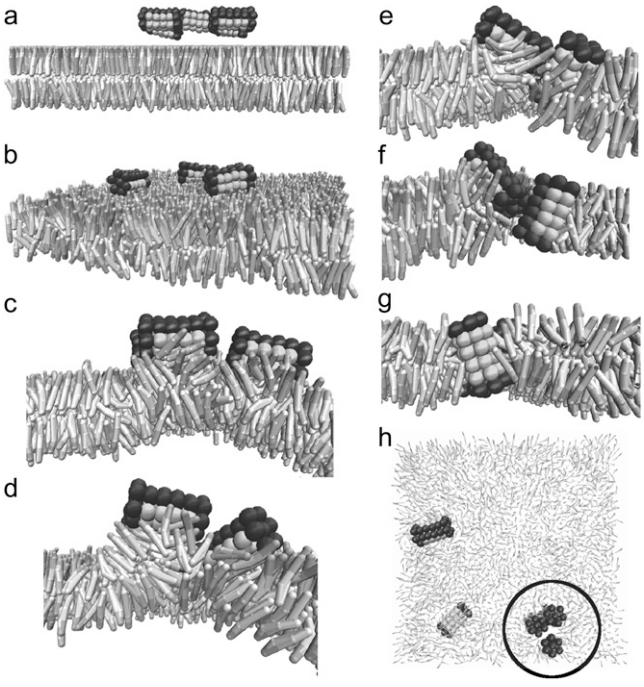


FIGURE 4 Cooperative insertion mechanism of several $P_6^2$ peptides ($\tilde{w}_c = 1.6$) at time steps (*a*) 0 $\tau$, (*b*) 250 $\tau$, (*c*) 14,750 $\tau$, (*d*) 15,500 $\tau$, (*e*) 15,750 $\tau$, (*f*) 17 250 $\tau$, and (*g*) 17,750 $\tau$. The top view in panel *h* at 17,750 $\tau$ shows that all three peptides have inserted and form a trimeric pore.

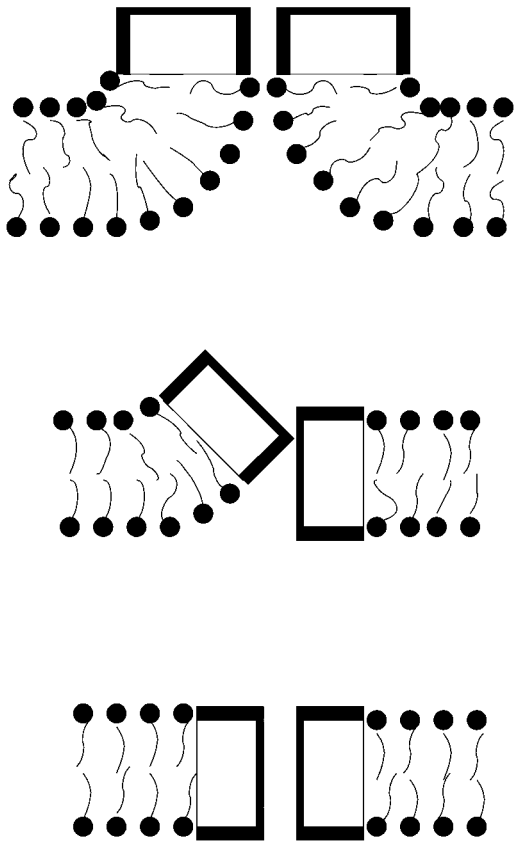

FIGURE 5 Sketch of a mechanism by which two peptides with a hydrophilic strip cooperatively insert into the bilayer, leaving a hydrophilic pathway.

we have extracted it from an inspection of our simulations. When two peptides with a hydrophilic strip bind next to each other on the bilayer surface, they strongly perturb the surrounding lipid structure, in particular by pulling lipid headgroups from the opposite leaflet toward their side. This facilitates the insertion of one of the peptides into the bilayer by shortening its breakthrough distance. While partially releasing the local bilayer disturbance, this rearrangement creates a hydrophilic path along the hydrophilic strip of the inserted peptide where the bilayer structure remains perturbed and along which the other peptide can slide down and likewise insert. We thus have two distinct reasons for cooperativity: 1), the joint bilayer perturbation is stronger, helping to overcome the energetic barrier for structural breach; and 2), once a peptide is inserted, it can help the second one to slide in. Of course, in reality these two effects are more difficult to disentangle as they often occur simultaneously.

As Fig. 4, *c* and *d*, clearly show, the bilayer perturbation caused by adhering APs involves a large number of lipids. Such collective rearrangements need to be distinguished from single lipid events (such as lipid flip-flop), and since collective rearrangements cause larger wavelength strains they might well involve lower total energies than single lipid events. Still, we want to emphasize at this point that the dynamics of flip-flop for the CG model we use is very much faster compared to real lipid bilayers (as we have quantified previously (30)). It is impossible to find a mapping of the CG time unit $\tau$ to seconds that gives both the correct long-time diffusion and the correct flip-flop rate. Stated differently, there is a mapping-independent way of comparing the dynamics of these two processes, namely, by stating how many lipid diameters a lipid will on average diffuse during an average flip-flop time. This distance is significantly larger in real membranes than in our CG model, essentially because the local solubilization of a single bilayer-embedded headgroup is energetically not very well represented. While it is unlikely that this affects our major conclusions about single particle insertion (that is, the existence of a threshold binding strength) and about the dominant mode of cooperative insertion (that is, taking advantage of the increased bilayer perturbation, in accord with (14), followed by the opening of an easy pathway once the first peptide has inserted), care must be exercised when interpreting the actual timescales involved.

## Pair correlation function of peptides without hydrophilic chains

### $P_8^0$ *peptides, comparing* $w_c = 1.5\,\sigma$ *and* $w_c = 1.7\,\sigma$

We begin by placing 40 $P_8^0$ peptides in a rectangular lattice, at $\sim 4\,\sigma$ above the bilayer surface, and compare the two peptide-lipid attractions $\tilde{w}_c = 1.5$ and $\tilde{w}_c = 1.7$. In the weaker interacting system, some of the peptides bind onto the bilayer surface while others diffuse away, but after $\sim 3000\,\tau$, all of them have inserted into the bilayer. This process can be noticed in a box size expansion during the early stage of simulation (total simulation time 75,000 $\tau$), reaching equilibrium a few 1000 $\tau$ after startup (Fig. 6). In the stronger interacting system, all peptides insert individually and much faster (at $\sim 750\,\tau$) into the bilayer. Since they compact their

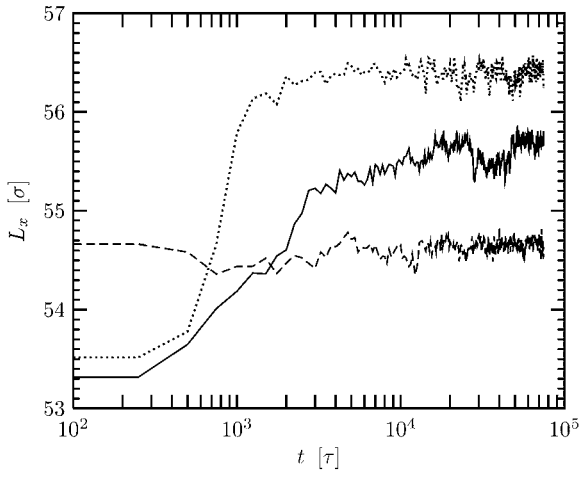


FIGURE 6 Box size expansion of 40 $P^0$ peptides with the following parameters: $P_8^0$, $\tilde{w}_c = 1.5$ (*solid*); $P_8^0$, $\tilde{w}_c = 1.7$ (*dashed*); and $P_6^0$, $\tilde{w}_c = 1.7$ (*dotted*).

peripheral lipids more strongly, the resulting equilibrium box size is smaller.

From the peptide pair correlation function $g(r)$ and a visual inspection of simulation snapshots (see *insets* in Fig. 7), we observe that the peptides with the stronger peptide-lipid attraction also tend to engage in a stronger local order. The strong lipid-peptide attraction causes the lipids to pack closely to the peptides, and this lipid shell in turn attracts neighboring peptides, thus forming a lipid bridge. It is possible that the attractions arise from an overlap of the lipid order parameter field surrounding the peptides (43–45): bringing two peptides together reduces the number of more highly ordered peripheral lipids, thereby increasing the overall entropy.

### *Comparison between $P_8^0$ and $P_6^0$ peptides*

To ensure a comparable amount of binding energy per peptide for the $P_8^0$ and the $P_6^0$ peptide species, we chose $\tilde{w}_c = 1.5$ for $P_8^0$ and $\tilde{w}_c = 1.7$ for $P_6^0$. We are thus asking the question how hydrophobic mismatch alone affects the peptide distribution.

As can be seen in Fig. 7, the peptide packing of the system with hydrophobic mismatch, $P_6^0$, is within the available statistics only marginally stronger than without hydrophobic mismatch, $P_8^0$. While mismatch can indeed lead to subtle pair interactions (46–48), such an effect cannot be uniquely identified in our case. Similar negative results have previously been reported in Monte Carlo simulations of proteins in lipid bilayers (49). In our study of a system of 40 $P_6^0$ peptides with the smallest value of peptide-lipid attraction at which peptides stay in the bilayer ($\tilde{w}_c = 1.6$), no tendency for peptide aggregation has been observed (data not shown). However, we can clearly notice that the mismatch-induced lipid tilt around the $P_6^0$ peptides expands the box stronger than in the non-tilt-inducing $P_8^0$ case (see again Fig. 6). In fact, in contrast to the tilt-free case, the stronger-bound peptides provoke—via tilt-splaying—a bigger box.

## Pore properties

After the cooperative insertion of two peptides, their hydrophilic strips face each other, which eliminates their contacts with lipid tails and thus partially restores an energetically favorable distribution of hydrophilic and hydrophobic residue contacts. However, such a peptide doublet has created a fully hydrophilic pathway through the bilayer. It cannot yet be termed a proper pore, but the local bilayer resistance to, say, ion permeation will certainly be impaired. Once more peptides join this local disturbance—in a process which is essentially the two-dimensional analog of the formation of inverted micelles (50)—the hydrophilic slit can open up to a genuine pore. In this section, we will study how the morphology of such pores depends on generic peptide properties, among them the strength of peptide-lipid interactions and the spatial distribution between hydrophilic and hydrophobic residues.

### *$P_8^2$ peptides, comparing $\tilde{w}_c = 1.5$ and $\tilde{w}_c = 1.7$*

Let us first discuss the influence of the peptide-lipid attraction on the pore/aggregate size. We study 40 $P_8^2$ peptides with either $\tilde{w}_c = 1.5$ or $\tilde{w}_c = 1.7$. These insert and form membrane pores—in the case $\tilde{w}_c = 1.5$ via the process explained in Cooperative Insertion Mechanism (above).

The presence of the hydrophilic chains makes the insertion process of the peptides with weak peptide-lipid attraction even more difficult. This can be seen in Fig. 8, which illus-

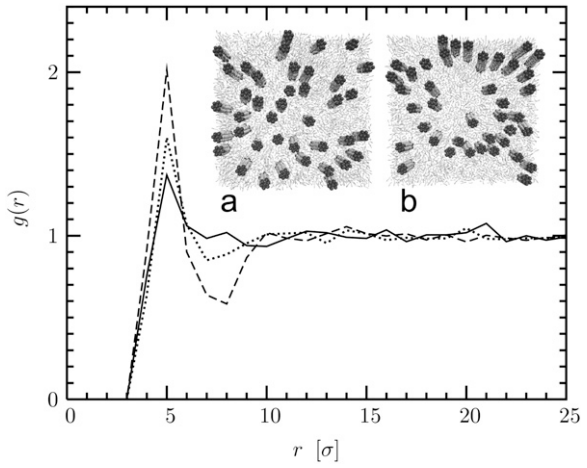


FIGURE 7 Pair correlation function $g(r)$ of 40 $P^0$ peptides with the following parameters: $P_8^0$, $\tilde{w}_c = 1.5$ (*solid*); $P_8^0$, $\tilde{w}_c = 1.7$ (*dashed*); and $P_6^0$, $\tilde{w}_c = 1.7$ (*dotted*). The two insets show snapshots of the two $P_8^0$ system with (*a*) $\tilde{w}_c = 1.5$ and (*b*) $\tilde{w}_c = 1.7$.

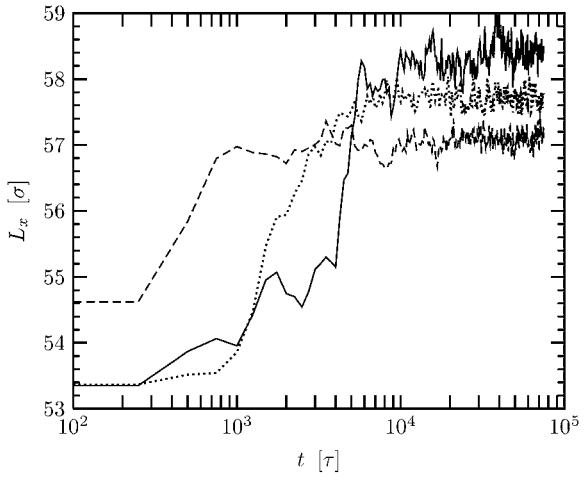


FIGURE 8 Box size expansion of 40 $P^2$ peptides with the following parameters: $P_8^2$, $\tilde{w}_c = 1.5$ (*solid*); $P_8^2$, $\tilde{w}_c = 1.7$ (*dashed*); and $P_6^2$, $\tilde{w}_c = 1.7$ (*dotted*).

trates that, compared to the strip-free $P^0$ peptides (Fig. 6), the time to reach an equilibrated box-size is longer.

The first thing to notice about the emerging pores is that their morphology resembles the model of toroidal pores (see Fig. 9). Individual peptides do not pack closely and form a rigid transmembrane cylinder; instead, they loosely stabilize the pore edge by reducing the line tension. Using density functional theory, Frink and Frischknecht have recently studied how this results in an optimal peptide spacing (51). We have confirmed (data not shown) that the line tension along such an open edge is lowered (and may even be rendered negative) upon the addition of such line-active molecules, for which the proper term ''linactant'' has recently been proposed (52,53). Importantly, in rim regions between peptides, the lipids curve between the two monolayers in a toroidal fashion, just as the toroidal pore model posits. From Fig. 9, *a* and *b*, we can also see that the pore sizes of the two $P_8^2$ systems ($\tilde{w}_c = 1.5$ and $\tilde{w}_c = 1.7$) are similar. Very roughly, pores consisting of 5–6 peptides are the most common, but there is a fair amount of fluctuation around this mean, as one would expect for low-energy transient structures. More statistics (more time and probably more peptides) would be needed to arrive at a full pore size distribution function.

At peptide-lipid attraction $\tilde{w}_c = 1.5$, the peptides first bind onto the bilayer surface, then cooperatively insert, and finally form larger pores by addition of interface or transmembrane single peptides. In contrast, at a peptide-lipid attraction $\tilde{w}_c = 1.7$, the strong attraction immediately drives the peptides to insert into the bilayer. This results in the presence of many single peptides or small peptide aggregates in the bilayer, which still exist after 75,000 $\tau$ ($\approx$750 $\mu$s) simulation time. Notice that this is sufficiently long to enable every peptide to diffuse across the entire membrane: their root-mean-square displacement is given by $\langle x^2 \rangle^{1/2} = 4Dt \simeq 4 \times 0.01\sigma^2/\tau \times 75,000\tau \simeq 55\sigma$. Since they individually bind more strongly to a pure bilayer, their merging with pores might energetically no longer be so favorable, but kinetic issues cannot be excluded at this point.

In the absence of explicit peptide-peptide attraction, we notice no evident interaction between the pores. Intuitively, from the previous result for $P_8^0$ peptides, one might have expected a weak attraction between pores composed of $P_8^2$ peptides. Yet, since the pore structure in this case has a toroidal arrangement, with the rim of the pore being formed by both lipids and peptides, the enhanced order imposed by the peptides is compensated by the reduced order of the splayed lipids at the open edge. Therefore, the overall order of lipids surrounding a pore may be not much different from the bulk, which would imply that an order-parameter-field-induced attraction cannot operate.

From oriented circular dichroism and neutron scattering techniques, a toroidal pore structure is indeed observed to occur with several APs, such as magainins, melittin, and protegrin peptides (8,18,19). For the case of melittin in a 1-palmitoyl-2-oleoyl-*sn*-glycero-3-phosphatidylcholine bilayer, evidence for toroidal lipid rearrangement has also been obtained recently in MD simulations (54). These authors have simulated the evolution of a pore constructed of, initially, four melittin peptides. It was found that lipid heads translocate from the rim to the central part of the interface, thereby making the interior of the pore hydrophilic and toroidally shaped. However, the very short simulation time of only 6 ns severely inhibits conclusions as to the optimal distribution of the melittins.

### *Comparison between $P_8^2$ and $P_6^2$ peptides*

We use the same two peptide species as in Comparison Between $P_8^0$ and $P_6^0$ Peptides to study the effect of hydrophobic mismatch on pore structure. Due to the presence of hydrophilic chains, the $P_6^2$ peptides are even more difficult to spontaneously insert into the bilayer than the $P_6^0$ peptides (compare again Figs. 6 and 8). None of the peptides insert spontaneously; they all require other peptides to catalyze the process. After insertion they form toroidal pores with 3–6 monomers per pore (see Fig. 9 *c*), but some smaller doublets or triplets still remain.

### *Pore size as a function of the number of hydrophilic chains*

As mentioned in the previous section, the presence of hydrophilic chains is necessary for pore formation, and the pore size grows until the hydrophilic chains are shielded from the hydrophobic lipid tails. Here we investigate how this process

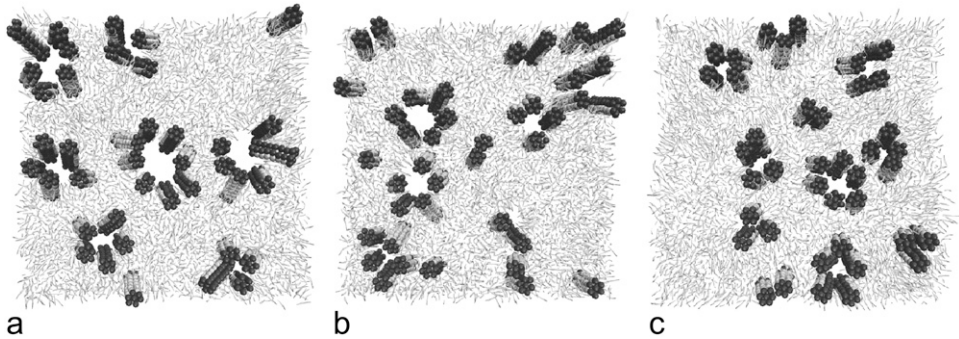


FIGURE 9 Pore formation of 40 $P^2$ peptides. The snapshots were taken after 75,000 $\tau$ and illustrate the following three systems: (*a*) $P_8^2$, $\tilde{w}_c = 1.5$; (*b*) $P_8^2$, $\tilde{w}_c = 1.7$; and (*c*) $P_6^2$, $\tilde{w}_c = 1.7$.

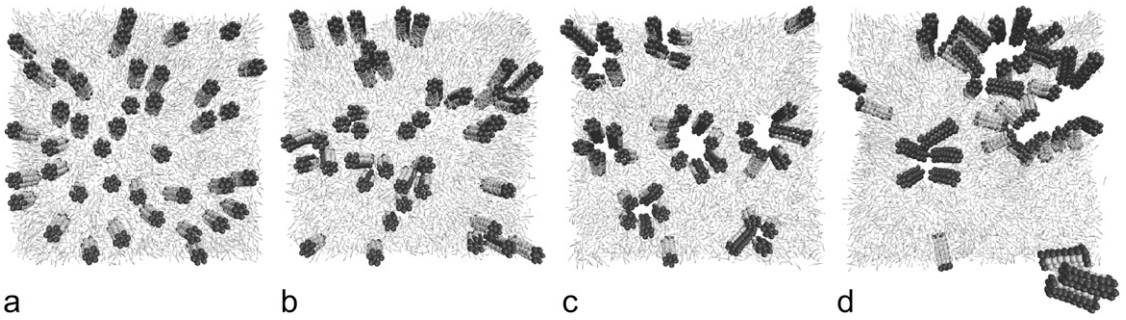


FIGURE 10 Pore formation of 40 $P_8^n$ peptides ($\bar{w}_c = 1.5$), differing in the number $n$ of hydrophilic strips. The snapshots were taken after 75,000 $\tau$ and illustrate the following four systems: (*a*) $P_8^0$; (*b*) $P_8^1$; (*c*) $P_8^2$; and (*d*) $P_8^3$.

depends on the size of the hydrophilic patch down the peptide length, i.e., on the number of hydrophilic chains.

As shown in Fig. 10 and in Table 3, the size of the pore grows as the number of hydrophilic strips is increased. This is in accord with recent theoretical modeling (50) and easily understood from the geometric constraint that after pore formation, peptides want to minimize the rim energy. They essentially act as two-dimensional surfactants at the bilayer-pore inter-line, and since they are not symmetric with respect to their own hydrophilic-hydrophobic distribution, they tend to induce a spontaneous curvature that in turn determines the pore size. The trend is such that a larger hydrophilic fraction also prefers larger pores.

However, one must be careful with this simple geometric picture, because it presupposes that all peptides indeed stay in the membrane. This is not necessarily easy for peptides with a large hydrophilic fraction, because their individual insertion (or even a cooperative pairwise process) is difficult. In other words, while peptides with a larger hydrophilic lining should be more toxic since they tend to form bigger pores, their initial insertion is also harder, which makes it more difficult for them to exercise their toxicity at low concentration. However, once a pore has formed, it can act as a nucleus for further peptide binding.

In Fig. 10 *c*, and particularly in Fig. 10 *d*, it is seen that several peptides are in the interface state. We have observed that these peptides sometimes evolve from a transmembrane state to an interface state and back to transmembrane state. This can results in an exchange of the peptides between neighboring pores, a process that could well be faster than if the peptide had to diffuse through the bilayer, even though this is very hard to quantify.

The increasing difficulty of peptide insertion with hydrophilicity (larger $n$ in $P_8^n$) is also seen in the time course of the box size expansion. Fig. 11 shows that increasing $n$ leads to a slower increase in $L_x$, even though the ultimate value is larger when $n$ is larger. Notice that the $P_8^3$ system also shows much bigger fluctuations in box size than all other systems. Indeed, these peptides' hydrophilic and hydrophobic faces have equal size, so that within the simple geometric picture one would expect zero spontaneous curvature of the stabilized bilayer rim—or in other words: infinite pores. Whether the finite pores in Fig. 10 *d* are just a kinetic intermediate or thermodynamically stable for more subtle reasons, it is clear that the bilayer is very close to structural failure, explaining the large variance in $L_x$. Given that in this system not even all $P_8^3$ peptides are bound to or inserted into the bilayer, even after 75,000 $\tau$, this is quite remarkable.

**TABLE 3 Rough guide of the most likely number of $P_8^n$ peptides forming a pore as a function of the number *n* of hydrophilic strips**

| Strips ($n$) | 0 | 1 | 2 | 3 |
|---|---|---|---|---|
| Pore size | No pore | 3–4 | 5–6 | $\gg$ |

### *Pore structure in the presence of peptide-peptide attraction*

As stated above, the process of peptide pore formation in bilayers is similar to micellization, driven by the hydrophilic-

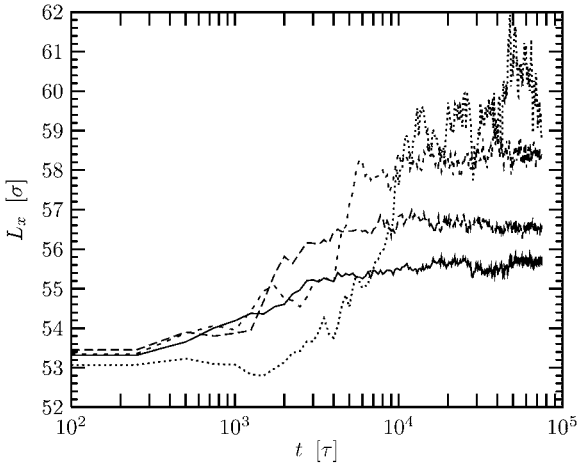


FIGURE 11 Box size of $P_8$ peptides with various number of hydrophilic chains and constant peptide-lipid attraction $\bar{w}_c = 1.5$. The box size increases as the number of hydrophilic chains increases. ($P_8^0$, *solid line*; $P_8^1$, *long-dashed line*; $P_8^2$, *short-dashed line*; and $P_8^3$, *dotted line*.) For the $P_8^3$ system, fluctuations between different runs were so large that no meaningful averaging could be performed. We therefore show—for this case only—the box-size trajectory of a single run during which the bilayer remained essentially intact.

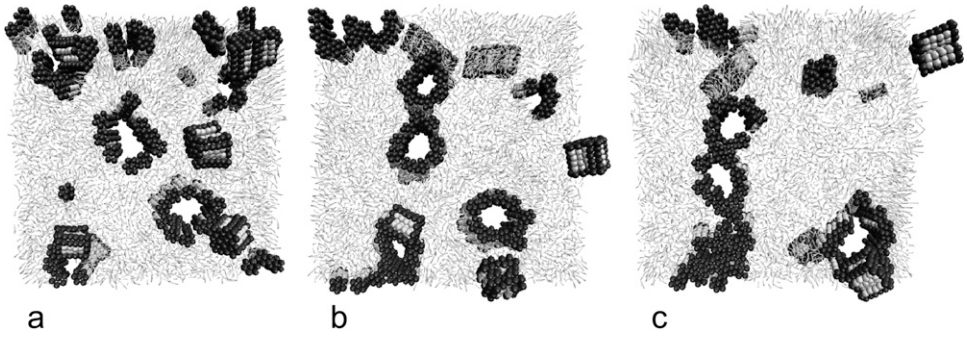


FIGURE 12 Time sequence of $P_6^2$ peptides with peptide-lipid and peptide-peptide cohesion $\tilde{w}_c = 1.6$. (*a*) Several pores are formed at 14,250 $\tau$. Notice their distinctly different morphology induced by peptide-peptide attractions, more reminiscent of the barrel-stave picture. (*b*) Two pores come close together at 34,000 $\tau$, but (*c*) do not coalesce even at 74,750 $\tau$.

hydrophobic distribution on the peptide's transmembrane surface. Introducing on top of that an explicit peptide-peptide attraction with the same potential as the peptide-lipid cohesion (here, $\tilde{w}_c = 1.6$) leads to a significantly different pore-morphology, as seen in the time sequence of Fig. 12. Not only do pores consist of more peptides, their mutual contact distance also shrinks to zero, such that there are no more lipids exposed at the inner pore surface. This shape resembles closely the picture of a barrel-stave arrangement, i.e., a transmembrane cylinder consisting exclusively of peptides forms the pore and all lipids around it are in a lamellar phase. Our simulations thus indicate that the interaction between peptides are very important in determining the pore morphology. This type of structure is observed for neutral peptides, such as alamethicin (16,17). Indeed, such APs would repel less than charged APs, thus being able to approach closer and form barrels, as has also been argued by Zemel et al. (50). Maybe even more importantly, our simulations show that in principle there is the possibility of a continuous transition between a more toroidlike and a more barrellike morphology, depending on the strength of the peptide-peptide interaction (which emerges from a subtle balance between hydrophobic, electrostatic, and fluctuation forces), such that not every antimicrobial peptide would need to unambiguously fall into one of the two classes.

Since peptides attract at close range, the interaction among the pores is also attractive. While we have seen two pores touching and sticking together, we have not observed their coalescence. It is very difficult to rule out kinetic traps in cases where such large energies are involved, but it should be pointed out that it is also not obvious that it must be a kinetic issue, because the argument of preferred spontaneous curvature still holds.

## CONCLUSIONS

Using coarse-grained MD simulations, we have observed the mechanism of cooperative peptide insertion into lipid bilayers, followed by pore formation if sufficiently many peptides are available. The presence of both hydrophilic caps and peptide-lipid attraction are essential to attract lipids and rearrange them into a structure which enables peptide insertion.

In the case of weak peptide-lipid attraction, individual peptides do not insert spontaneously but need other peptides to catalyze this process—by both increasing the bilayer deformation and providing an easy-insertion pathway. This autocatalytic mechanism may explain the experimental finding of a cooperative concentration dependence of antimicrobial peptides activity: only when the peptide/lipid concentration increases above a certain threshold value, the peptides change their state from interface to transmembrane (6,8,11,13). We observe that in the case of strong peptide-lipid attraction, the peptides can spontaneously insert into the bilayer. However, in this case their tendency to form large pores seems diminished. Furthermore, a strong insertion energy implies that the peptides are very hydrophobic and thus not well soluble in water. It is then unclear how they would easily get to the membrane of the pathogen they are supposed to destroy. A more successful strategy is thus to have peptides which are better soluble and which just about insert into the membrane with the cooperative help of others, but which subsequently have a tendency to aggregate into larger pores.

In our system, the difference between a toroidal and a barrel-stave pore structure is found to be dependent on the direct peptide-peptide interaction. If peptides strongly attract, they completely close up at the membrane-pore boundary and thus assume a barrel-stave geometry. Conversely, if peptide attraction is sufficiently small, they behave as linactants and merely stabilize a toroidal rim at the membrane-pore edge. It is clear, however, that these two scenarios are only the endpoints of a continuum of pore morphologies and that real antimicrobial peptides may show properties in-between.

We have seen in various examples that very generic features of the peptide have clear effects on the peptide-membrane interaction, the insertion process, and the subsequent pore morphology. Attempting to isolate them in the way proposed here may guide our attempts to design synthetic channel-forming peptides as a new artificial line of defense against various pathogens.

We enjoyed many clarifying discussions with B. Reynwar, C. Peter, D. Andrienko, B. Dünweg, and K. Kremer.

M.D. also acknowledges financial support by the German Science Foundation under grant No. De775/1-3.

## REFERENCES


1. Zasloff, M. 1987. Magainins, a class of antimicrobial peptides from *Xenopus* skin—isolation, characterization of two active forms, and partial Cdna sequence of a precursor. *Proc. Natl. Acad. Sci. USA.* 84:5449–5453.
2. Gesell, J., M. Zasloff, and S. Opella. 1997. Two-dimensional H-1 NMR experiments show that the 23-residue magainin antibiotic peptide is an $\alpha$-helix in dodecylphosphocholine micelles, sodium dodecylsulfate micelles, and trifluoroethanol/water solution. *J. Biomol. NMR.* 9:127–135.
3. Habermann, E. 1972. Bee wasp venoms. *Science.* 177:314–322.
4. Hall, J. E., I. Vodyanoy, T. M. Balasubramanian, and G. R. Marshall. 1984. Alamethicin—a rich model for channel behavior. *Biophys. J.* 45:233–247.
5. Huang, H. W. 2006. Molecular mechanism of antimicrobial peptides: the origin of cooperativity. *Biochim. Biophys. Acta.* 1758:1292–1302.
6. Matsuzaki, K., K. Sugishita, N. Ishibe, M. Ueha, S. Nakata, K. Miyajima, and R. M. Epand. 1998. Relationship of membrane curvature to the formation of pores by magainin 2. *Biochemistry.* 37:11856–11863.
7. Pouny, Y., D. Rapaport, A. Mor, P. Nicolas, and Y. Shai. 1992. Interaction of antimicrobial dermaseptin and its fluorescently labeled analogs with phospholipid-membranes. *Biochemistry.* 31:12416–12423.
8. Yang, L., T. A. Harroun, T. M. Weiss, L. Ding, and H. W. Huang. 2001. Barrel-stave model or toroidal model? A case study on melittin pores. *Biophys. J.* 81:1475–1485.
9. Huang, H. W. 2000. Action of antimicrobial peptides: two-state model. *Biochemistry.* 39:8347–8352.
10. Bechinger, B., Y. Kim, L. E. Chirlian, J. Gesell, J.-M. Neumann, M. Montal, J. Tomich, M. Zasloff, and S. J. Opella. 1991. Orientations of amphipathic helical peptides in membrane bilayers determined by solid-state NMR spectroscopy. *J. Biomol. NMR.* 1:167–173.
11. Wieprecht, T., O. Apostolov, M. Beyermann, and J. Seelig. 2000. Membrane binding and pore formation of the antibacterial peptide PGLA: thermodynamic and mechanistic aspects. *Biochemistry.* 39: 442–452.
12. Zemel, A., A. Ben-Shaul, and S. May. 2004. Membrane perturbation induced by interfacially adsorbed peptides. *Biophys. J.* 86:3607–3619.
13. Longo, M. L., A. J. Waring, L. M. Gordon, and D. A. Hammer. 1998. Area expansion and permeation of phospholipid membrane bilayers by influenza fusion peptides and melittin. *Langmuir.* 14:2385–2395.
14. Zemel, A., A. Ben-Shaul, and S. May. 2005. Perturbation of a lipid membrane by amphipathic peptides and its role in pore formation. *Eur. Biophys. J.* 34:230–242.
15. Wu, M. H., E. Maier, R. Benz, and R. E. W. Hancock. 1999. Mechanism of interaction of different classes of cationic antimicrobial peptides with planar bilayers and with the cytoplasmic membrane of *Escherichia coli*. *Biochemistry.* 38:7235–7242.
16. Matsuzaki, K., M. Harada, T. Handa, S. Funakoshi, N. Fujii, H. Yajima, and K. Miyajima. 1989. Magainin 1-induced leakage of entrapped calcein out of negatively-charged lipid vesicles. *Biochim. Biophys. Acta.* 981:130–134.
17. He, K., S. J. Ludtke, D. L. Worcester, and H. W. Huang. 1996. Neutron scattering in the plane of membranes: structure of alamethicin pores. *Biophys. J.* 70:2659–2666.
18. Matsuzaki, K., O. Murase, N. Fujii, and K. Miyajima. 1996. An antimicrobial peptide, magainin 2, induced rapid flip-flop of phospholipids coupled with pore formation and peptide translocation. *Biochemistry.* 35:11361–11368.
19. Ludtke, S. J., K. He, W. T. Heller, T. A. Harroun, L. Yang, and H. W. Huang. 1996. Membrane pores induced by magainin. *Biochemistry.* 35:13723–13728.
20. Leontiadou, H., A. E. Mark, and S. J. Marrink. 2006. Antimicrobial peptides in action. *J. Am. Chem. Soc.* 128:12156–12161.
21. Lopez, C. F., S. O. Nielsen, P. B. Moore, and M. L. Klein. 2004. Understanding nature's design for a nanosyringe. *Proc. Natl. Acad. Sci. USA.* 101:4431–4434.
22. Lopez, C. F., S. O. Nielsen, B. Ensing, P. B. Moore, and M. L. Klein. 2005. Structure and dynamics of model pore insertion into a membrane. *Biophys. J.* 88:3083–3094.
23. Lopez, C. F., S. O. Nielsen, G. Srinivas, W. F. DeGrado, and M. L. Klein. 2006. Probing membrane insertion activity of antimicrobial polymers via coarse-grain molecular dynamics. *J. Chem. Theory Comput.* 2:649–655.
24. Venturoli, M., B. Smit, and M. M. Sperotto. 2005. Simulation studies of protein-induced bilayer deformations, and lipid-induced protein tilting, on a mesoscopic model for lipid bilayers with embedded proteins. *Biophys. J.* 88:1778–1798.
25. Brannigan, G., and F. L. H. Brown. 2007. Contributions of Gaussian curvature and nonconstant lipid volume to protein deformation of lipid bilayers. *Biophys. J.* 92:864–876.
26. Monticelli, L., S. K. Kandasamy, X. Periole, R. G. Larson, D. P. Tieleman, and S. J. Marrink. 2008. The MARTINI coarse-grained force field: extension to proteins. *J. Chem. Theory Comput.* 4:819–834.
27. Müller, M., K. K., and M. Schick. 2006. Biological and synthetic membranes: what can be learned from a coarse-grained description? *Phys. Rep.* 434:113–176.
28. Venturoli, M., M. M. Sperotto, M. Kranenburg, and B. Smit. 2006. Mesoscopic models of biological membranes. *Phys. Rep.* 437: 1–54.
29. Cooke, I. R., K. Kremer, and M. Deserno. 2005. Tunable generic model for fluid bilayer membranes. Part 1. *Phys. Rev. E Stat. Nonlin. Soft Matter Phys.* 72:011506.
30. Cooke, I. R., and M. Deserno. 2005. Solvent-free model for self-assembling fluid bilayer membranes: stabilization of the fluid phase based on broad attractive tail potentials. *J. Chem. Phys.* 123:224710.
31. Brannigan, G., L. C. L. Lin, and F. L. H. Brown. 2006. Implicit solvent simulation models for biomembranes. *Eur. Biophys. J.* 35:104–124.
32. Cooke, I. R., and M. Deserno. 2006. Coupling between lipid shape and membrane curvature. *Biophys. J.* 91:487–495.
33. Harmandaris, V. A., and M. Deserno. 2006. A novel method for measuring the bending rigidity of model lipid membranes by simulating tethers. *J. Chem. Phys.* 125:204905.
34. Reynwar, B. J., G. Illya, V. A. Harmandaris, M. M. Müller, K. Kremer, and M. Deserno. 2007. Aggregation and vesiculation of membrane proteins by curvature-mediated interactions. *Nature.* 447:461–464.
35. Kechuan, T., D. J. Tobias, and M. L. Klein. 1995. Constant pressure and temperature molecular dynamics simulation of a fully hydrated liquid crystal phase dipalmitoylphosphatidylcholine bilayer. *Biophys. J.* 69:2558–2562.
36. Hess, B., S. León, N. van der Vegt, and K. Kremer. 2007. Long time atomistic polymer trajectories from coarse grained simulations: bisphenol-A polycarbonate. *Soft Matter.* 2:409–414.
37. Harmandaris, V. A., N. P. Adhikari, N. F. A. van der Vegt, K. Kremer, B. A. Mann, R. Voelkel, H. Weiss, and C. C. Liew. 2007. Ethylbenzene diffusion in polystyrene: united atom atomistic/coarse-grained simulations and experiments. *Macromolar.* 40:7026–7035.
38. Limbach, H. J., A. Arnold, B. A. Mann, and C. Holm. 2006. ESPResSo—an extensible simulation package for research on soft matter systems. *Comput. Phys. Commun.* 174:704–727.
39. Grest, G. S., and K. Kremer. 1986. Molecular-dynamics simulation for polymers in the presence of a heat bath. *Phys. Rev. A.* 33:3628–3631.
40. Kolb, A., and B. Dünweg. 1999. Optimized constant pressure stochastic dynamics. *J. Chem. Phys.* 111:4453–4459.
41. Humphrey, W., A. Dalke, and K. Schulten. 1996. VMD—visual molecular dynamics. *J. Mol. Graph.* 14:33–38.
42. Reynolds, J. A., D. B. Gilbert, and C. Tanford. 1974. Empirical correlation between hydrophobic free energy and aqueous cavity surface area. *Proc. Natl. Acad. Sci. USA.* 71:2925–2927.
43. Marcelja, S. 1976. Lipid-mediated protein interaction in membranes. *Biochim. Biophys. Acta.* 455:1–7.

44. Jähnig, F. 1981. Critical effects from lipid-protein interaction in membranes. *Biophys. J.* 36:329–345.

45. Sintes, T., and A. Baumgärtner. 1997. Protein attraction in membranes induced by lipid fluctuations. *Biophys. J.* 73:2251–2259.

46. Dan, N., P. Pincus, and S. A. Safran. 1993. Membrane-induced interactions between inclusions. *Langmuir.* 9:2768–2771.

47. Dan, N., A. Berman, P. Pincus, and S. A. Safran. 1994. Membrane-induced interactions between inclusions. *J. Phys. II* (*France*). 4:1713–1725.

48. Aranda-Espinoza, H., A. Berman, N. Dan, P. Pincus, and S. A. Safran. 1996. Interactions between inclusions embedded in membranes. *Biophys. J.* 71:648–656.

49. Sperotto, M. M., and O. G. Mouritsen. 1991. Mean-field and Monte Carlo simulation studies of the lateral distribution of proteins in membranes. *Eur. Biophys. J.* 19:157–168.

50. Zemel, A., D. R. Fattal, and A. Ben-Shaul. 2003. Energetics and self-assembly of amphipathic peptide pores in lipid membranes. *Biophys. J.* 84:2242–2255.

51. Frink, L. J. D., and A. L. Frischknecht. 2006. Computational investigations of pore forming peptide assemblies in lipid bilayers. *Phys. Rev. Lett.* 97:208701.

52. Panda, A. K., K. Nag, R. R. Harbottle, F. Possmayer, and N. O. Petersen. 2007. Thermodynamic studies of bovine lung surfactant extract mixing with cholesterol and its palmitate derivative. *J. Colloid Interface Sci.* 311:551–555.

53. Trabelsi, S., S. Zhang, T. R. Lee, and D. K. Schwartz. 2008. Linactants: surfactant analogues in two dimensions. *Phys. Rev. Lett.* 100:037802.

54. Lin, J.-H., and A. Baumgaertner. 2000. Stability of a melittin pore in a lipid bilayer: a molecular dynamics study. *Biophys. J.* 78:1714–1724.